

Two-Way Molecular Communications

Jong Woo Kwak, *Student Member, IEEE*, H. Birkan Yilmaz, *Member, IEEE*, Nariman Farsad, *Member, IEEE*, Chan-Byoung Chae, *Senior Member, IEEE*, and Andrea Goldsmith, *Fellow, IEEE*

Abstract—For nano-scale communications, there must be cooperation and simultaneous communication between nano devices. To this end, in this paper, we investigate two-way (a.k.a. bi-directional) molecular communications between nano devices. If different types of molecules are used for the communication links, the two-way system eliminates the need to consider self-interference. However, in many systems, it is not feasible to use a different type of molecule for each communication link. Thus, we propose a two-way molecular communication system that uses a single type of molecule. We derive a channel model for this system and use it to analyze the proposed system’s bit error rate, throughput, and self-interference. Moreover, we propose analog- and digital- self-interference cancellation techniques. The enhancement of link-level performance using these techniques is confirmed with both particle-based simulations and analytical results.

Index Terms—Molecular communication, two-way communication, and self-interference cancellation.

I. INTRODUCTION

OVER the past decade, developments in the field of nanorobotics have enabled the use of nano devices in various technologies and especially in those used by the bio-medical industry [2]–[6]. Well-organized clusters of nano devices can be used for drug delivery applications and artificial immune systems. Each cluster is responsible for a single task, e.g., discovering or destroying of pathogens. Since a nano device can only perform simple tasks, it is important to have a communication system among nano devices. Radio frequency (RF)-based communication is not suitable for nano devices because of physical limitations such as the size of the antenna, which is typically proportional to the wavelength of the electromagnetic (EM) wave in order to maximize efficiency [7], [8]. Furthermore, EM waves—especially at high frequencies—do not propagate well in the body [9].

Thus, researchers have focused on molecular communication as an alternative to RF-based communication, where information is transmitted via molecules. One such system is that of molecular communication via diffusion (MCvD). Here molecules are propagated in an environment by diffusion [10].

J. Kwak and C.-B. Chae are with the School of Integrated Technology, Yonsei University, Korea. H. B. Yilmaz was with the School of Integrated Technology, Yonsei University, Korea, and now he is with the Dept. of Network Engineering, Polytechnic University of Catalonia, Spain. N. Farsad and A. Goldsmith are with the Department of Electrical Engineering, Stanford University, USA.

This research was supported in part by the MSIT (Ministry of Science and ICT), Korea, under the ICT Consilience Creative program (IITP-2017-2017-0-01015), the BA-SIC Science Research Program (2017R1A1A1A05001439) through the National Research Foundation of Korea, the Government of Catalonia’s Secretariat for Universities and Research via the Beatriu de Pinós postdoctoral program, and the NSF Center for Science of Information (CSoI) under grant CCF-0939370.

Part of this work is presented in [1].

An MCvD system mainly consists of the following: transmitter nodes capable of emitting and modulating information through molecules, receiver nodes capable of receiving and demodulating molecular signals, information molecules to transfer information, and a fluid environment to host nodes and molecules. Physical realization of the transceiver is also an important issue. The authors in [11], [12] used Quorum Sensing [13] to synchronize the activities of a cluster of engineered bacteria implemented on a chip. Using this orchestrated bacteria cluster as a node, the authors in [14] proposed a diffusion-based molecular communication network.

One of the main challenges in MCvD is to establish channel models for representing the molecular received signal (i.e., a time-dependent solution of the fraction of received molecules by time t). Some known channel models assume that the arrival time of molecules are a first-passage time process (i.e., information molecules are absorbed whenever they hit a receiver) [15]–[19]. Compared to the case of transparent receivers, using the absorbing receiver makes it hard to derive the channel model due to the additional boundary condition. In this paper, we consider the absorbing receivers. The authors in [18] modeled the molecular received signal in a three-dimensional (3-D) environment— a point source represented a transmitter, and an absorbing sphere represented a receiver. For this basic topology, it is possible to acquire an analytical closed form of the channel model representing the molecular received signal due to spherical symmetry. If the system has more than one absorbing sphere (receiver), however, such symmetry disappears. It is then difficult to model the arrival times mathematically.

Other challenges in MCvD include low transmission rates due to severe inter-symbol interference (ISI). In MCvD, ISI occurs when the molecules of a previous symbol are absorbed by the target receiver in the current or future symbol slots. The heavy tail nature of impulse responses in MCvD causes severe ISI. Thus, several researchers [20], [21] have suggested ISI mitigation techniques, including enzymatic degradation of ISI using different molecule types. All of these works assumed a one-way MCvD system whereby molecules are transmitted in one direction from the transmitter to the receiver. While this simplifies the design, recent work in full-duplex radio communications [22]–[24] indicates that data rate gains along with other performance advantages may be obtained from two-way communication.

In this paper, we propose a two-way MCvD system that uses a *single* type of molecule for simultaneous communication between two nano devices. If each of the directional communication links uses a different type of molecule, then

self-interference¹ (SI) will not occur [25]–[27]. However, this is not a feasible solution. First, the nano devices are too simple to perform complex tasks and, second, the number of molecule types will increase rapidly, on the order of $\binom{\ell}{2}$ where ℓ is the number of communication links. Therefore, we propose a two-way MCvD system that uses a single type of molecule for each link. Two communication models—a half-duplex system and a full-duplex system—are considered. In the half-duplex system, each paired transceiver (i.e., for Rx_1 , the paired transmitter is Tx_2) operates alternately with respect to time. In the full-duplex system, each paired transceiver operates simultaneously with respect to time (i.e., it is not necessary to wait until the other transceiver ends its communication). However, the analytical modeling of such a system is not without difficulty—two absorbing spheres are to use a single type of molecule. Unfortunately, to implement simultaneous communication between two nano devices, we cannot use previous studies on MCvD channel models as such studies assumed a one-way MCvD system with a single absorbing sphere. Therefore, in this paper, we analytically model the molecular received signal in the case of two absorbing spheres, propose SI cancellation (SIC) techniques, and analyze the proposed system’s performance in terms of bit error rate (BER) and throughput. The main contributions of this paper are as follows:

- The channel model of a two-way MCvD system with two absorbing sphere receivers is derived. To the best of our knowledge, it is the first work that derives the channel model for multi absorbing receiver case. We improve the channel model derived in [1]. More precisely, we analytically derive the asymptotic capture probability (i.e., the probability that the molecules eventually being absorbed by the receivers). By using the derived asymptotic capture probability, we also derive an approximation of the time-dependent solution of the fraction of the received molecules by time t . The derived channel model is validated through particle-based simulations.
- The paper derives the BER expression for two two-way MCvD systems—one with a half-duplex system and one with a full-duplex system. The theoretical BERs are then validated through particle-based simulations.
- The paper proposes two SIC techniques—analogue SI cancellation (A-SIC) and digital SI cancellation (D-SIC)—as analytical results show that it is impossible to achieve reliable data transmission without SIC in the full-duplex system. Using the derived channel model and the BER expression, we investigate the optimal values for the normalized detection threshold and the discarding time (i.e., initial part of the received signal is ignored by discarding time T_c) in order to minimize the BER. The throughputs and BERs of both systems are analyzed. We compare the SIC-adopted full-duplex system with binary concentration shift keying (BCSK) to the half-duplex system with quadrature concentration shift keying

¹Self-interference in MCvD refers to a phenomenon in which a molecule emitted from the transmitter is absorbed by its own rather than the intended receiver.

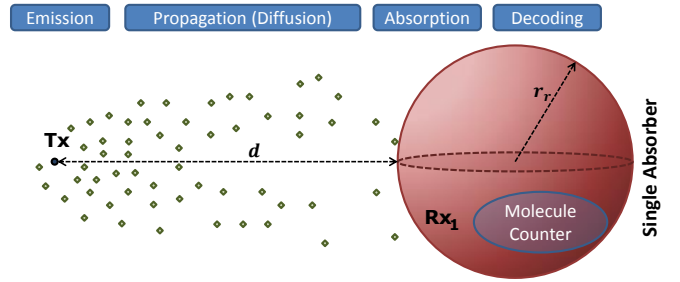


Fig. 1. Conventional one-way MCvD transceiver model and the processes with a point transmitter (Tx) and an absorbing sphere (Rx_1).

(QCSK), which is not provided in [1].

The rest of this paper is organized as follows. In Section II, we discuss the conventional one-way MCvD model. In Section III, we introduce the proposed two-way MCvD system and SIC techniques. In Section IV, we investigate the channel model of a two-way MCvD system with two absorbing sphere receivers. Then we present the channel model verifications and BER formulations for the two considered systems. In Section V, we present performance analysis results in terms of BER and throughput for the two considered systems. Finally, in Section VI, we present our conclusions.

II. ONE-WAY MOLECULAR COMMUNICATION

We start by providing details of the conventional one-way MCvD system. Also, we present details of the single absorbing receiver channel model so that the reader may understand the differences and challenges with respect to the corresponding model for two-way molecular communication system.

A. Conventional one-way MCvD system

The conventional one-way MCvD system consists of a point source (point transmitter) and an absorbing sphere (receiver). In Fig. 1, the point source (point transmitter), Tx , is separated from the absorbing sphere (receiver), Rx_1 , the radius of which is denoted by r_r , by a distance of d . Here we focus on three molecular processes: emission, propagation, and reception. The emission process is related to the modulation of the data bits onto the physical properties of the molecules or the emission time [28]. The propagation process is governed by diffusion and flow [29]–[31]. In this paper, we only consider diffusion. The reception process is related to the acquisition of the molecules at the receiver and the demodulation of the data bits.

Regarding the propagation process, the interactions between diffusing molecules are ignored since the messenger molecules are assumed to be chemically stable. We assume that the transmitter and the receiver are fully synchronized, which can be achieved by the method introduced in [32].

B. Channel Model for One-way Molecular Communication with a Single Receiver

In diffusion-based systems, propagation of the molecules is governed by Fick's second law in a 3-D environment; that is

$$\frac{\partial p(r, t|r_0)}{\partial t} = D\nabla^2 p(r, t|r_0), \quad (1)$$

where ∇^2 , $p(r, t|r_0)$, and D are the Laplacian operator, the molecule distribution function at time t and distance r given the initial distance r_0 , and the diffusion constant, respectively. The value of D depends on the temperature, viscosity of the fluid, and the Stokes radius of the molecule [33].

Fig. 1 illustrates a simple topology of one-way MCvD. In [18], the expected channel response of one-way MCvD is presented and analyzed from a channel characteristics perspective. Also, a time-dependent solution for a fraction of molecules hitting a single absorbing sphere (Rx_1) by time t is presented, as follows:

$$\begin{aligned} G_1^{\text{Tx}}(t) &= \int_0^t g_1^{\text{Tx}}(t') dt' \\ &= \int_0^t \frac{r_r}{r_r+d} \frac{d}{\sqrt{4\pi Dt'^3}} e^{-d^2/4Dt'} dt' \\ &= \frac{r_r}{r_r+d} \operatorname{erfc}\left(\frac{d}{\sqrt{4Dt}}\right), \end{aligned} \quad (2)$$

where Tx , $g_1^{\text{Tx}}(t)$, r_r , d , and $\operatorname{erfc}(\cdot)$ represent the location of the point transmitter, the instantaneous hitting probability density (i.e., the arrival time distribution for Rx_1 when the molecules are emitted from Tx), the radius of the receiver, the distance from Tx to Rx_1 , and the complementary error function, respectively.

III. TWO-WAY MOLECULAR COMMUNICATION

In this section, we introduce two modes of operation for the proposed two-way MCvD system, i.e., full-duplex and half-duplex based on time-division. In the former case, severe SI is observed when both transceivers simultaneously modulate signals using the same type of molecule. Therefore, in this case, it is necessary to apply an SIC technique.

A. Topology

We consider a 3-D environment with two point sources (transmitters) and two absorbing spheres (receivers). Each transmitter emits molecules without directionality. The propagation of molecules is governed by (1). The molecules are immediately absorbed when they reach the surface of any one of the receivers. Since the absorbed molecules are removed from the system, each molecule is detected at most once.

Fig. 2 shows the model of the proposed system. The blue pipes in Fig. 2 represent the connection between the transmitting part and the receiving part. They are assumed to be transparent to the released molecules. Tx_i releases molecules that are intended to be absorbed by Rx_j ($i \neq j$). If the molecules that are released from Tx_i are absorbed by Rx_i (not the desired result), then we call this SI. The distance between Tx_i and Rx_i is denoted by d_i , and the distance from a point p to Rx_j is denoted by $d_p^{\text{Rx}_j}$.

The system model illustrated in Fig. 2 is similar to full duplex radios with RF technologies that have antenna separation as passive analog cancellation and digital self interference cancellation. We leave the fabrication issues for the transceivers for our future work and will focus on fundamental analyses of the proposed system.

B. Communication Model & Modulation

Consider the following two modes of operation for the proposed two-way MCvD system:

- Half-duplex system: Tx_1 and Tx_2 release molecules alternately (i.e., when Tx_1 emits molecules, Rx_1 and Rx_2 receive the molecules but Rx_1 does not count the molecules).
- Full-duplex system: Tx_1 and Tx_2 release molecules simultaneously that are intended for Rx_2 and Rx_1 , respectively. Receiver Rx_i receives and counts the molecules that are emitted by Tx_i and Tx_j .

In the half-duplex system, at least half of the elements of the bit sequences are not used (i.e., Tx_1 does not emit molecules when Tx_2 emits molecules), which is not the case for the full-duplex system. Therefore, the ISI and the SI are much more severe in the full-duplex system. For the n th symbol period, the molecular received signal is composed of $2n$ bits including the current symbols and the previous $2n-2$ symbols sent from the two transmitters. The bit sequences for the transmitters are denoted by $x_1[1:n]$ and $x_2[1:n]$.

For the modulation, we use binary/quadrature concentration shift keying (BCSK, QCSK) [28]. We let N_1 denote the number of molecules for encoding bit-1, and we define that there will be no emission in the case of bit-0 for BCSK. Each of the transmitters has its bit sequences x_i to encode, where $x_i[k]$ denotes the symbol in the k th symbol duration for Tx_i . We define $P_{ij}[k]$ as the probability that molecules emitted from Tx_i hit Rx_j in the k th symbol duration after the emission, which is formulated as follows:

$$P_{ij}[k] \triangleq P_{ij}(kt_s, (k+1)t_s), \quad k \in \mathbb{N}_0, \quad (3)$$

where t_s and $P_{ij}(t_1, t_2)$ denote the symbol duration and the probability that molecules emitted from Tx_i are absorbed by Rx_j but not Rx_i between time t_1 and t_2 after the emission. In the rest of this paper we call $P_{ij}[k]$ the channel coefficient.

In (3), $P_{ij}[0]$ corresponds to the probability of being absorbed in the current symbol slot. We let $y_{\text{Rx}_j}[n]$ denote the number of molecules that are absorbed by Rx_j in the n th symbol slot. Note that $y_{\text{Rx}_j}[n]$ can be affected by the number of molecules released from (i) a pair source at the current symbol slot, (ii) a pair source at the previous time slots, (iii) a non pair source at the current symbol slot, and (iv) non pair source at the previous time slots. To formulate $y_{\text{Rx}_j}[n]$, we define $N_{ij}[k]$ as follows:

$$N_{ij}[k] \sim \mathcal{B}(N_1, P_{ij}[k]), \quad (4)$$

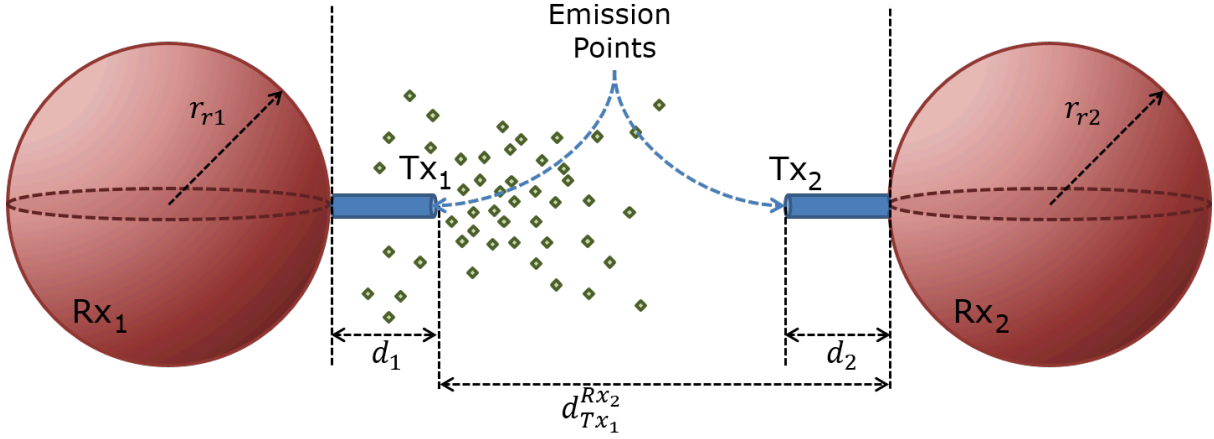


Fig. 2. Model for two-way MCvD system featuring two transmitters (i.e., Tx₁ and Tx₂) and two receivers (i.e., Rx₁ and Rx₂).

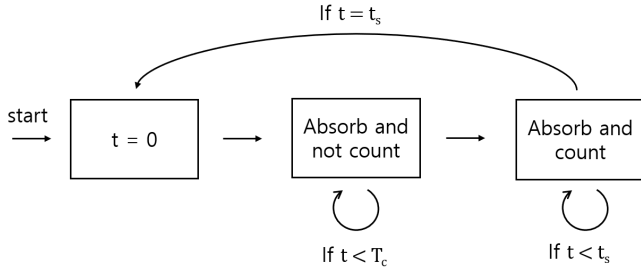


Fig. 3. State diagram of the process of A-SIC. For each symbol slot, the absorbed molecules are discarded by $t = T_c$.

where $\mathcal{B}(m, p)$ is a binomial distribution with m trials and success probability p . Then, $y_{\text{Rx}_j}[n]$ can be formulated as follows:

$$y_{\text{Rx}_j}[n] \triangleq \sum_{k=0}^{n-1} (N_{ij}[k] \cdot x_i[n-k] + \underbrace{N_{jj}[k] \cdot x_j[n-k]}_{\text{self-interference}}) + s[n]. \quad (5)$$

To consider the misoperations of the receiver, we add the noise term which is assumed to be a Gaussian random variable, $s[n] \sim \mathcal{N}(0, \sigma_{\text{noise}}^2)$. For the sake of tractability, we approximate the binomial distribution as follows:

$$N_{ij}[k] \approx \mathcal{N}(N_1 P_{ij}[k], N_1 P_{ij}[k](1 - P_{ij}[k])), \quad (6)$$

where $\mathcal{N}(\mu, \sigma^2)$ represents a Gaussian distribution with mean μ and variance σ^2 . Hence, $y_{\text{Rx}_j}[n]$ can be expressed as follows (i.e., as a Gaussian random variable, where mean and variance values are dependent upon transmitted bit sequences):

$$\begin{aligned} y_{\text{Rx}_j}[n] &\sim \mathcal{N}(\mu_{n,\text{total}}, \sigma_{n,\text{total}}^2) \\ \mu_{n,\text{total}} &= \sum_{k=0}^{n-1} N_1 (P_{ij}[k] x_i[n-k] + P_{jj}[k] x_j[n-k]) \\ \sigma_{n,\text{total}}^2 &= \sigma_{\text{noise}}^2 + \sum_{k=0}^{n-1} N_1 (P_{ij}[k](1 - P_{ij}[k]) x_i[n-k] \\ &\quad + P_{jj}[k](1 - P_{jj}[k]) x_j[n-k]). \end{aligned} \quad (7)$$

C. Self-Interference Cancellation

Since the proposed two-way MCvD system comprises two transceivers that use the same type of molecule, the system's receivers are unable to distinguish molecules in terms of the transmitting source. For example, if Tx₁ sends bit-1 and Tx₂ sends bit-0, the molecules are released only from Tx₁. However, those molecules can also be absorbed by Rx₁, which is not desired. Then Rx₁ may decode the received signal as bit-1, even though its paired transmitter Tx₂ sends bit-0. In fact, most of the molecules released from Tx₁ will be absorbed by Rx₁ because Tx₁ is much closer to Rx₁ than Rx₂. Hence, in this case, the number of received molecules is mostly dependent on the transmitted symbol from the unpaired transmitter, which makes for infeasible communication. Therefore, we propose the following two SIC techniques:

- Analog self-interference cancellation (A-SIC): the initial part (i.e., between time 0 and T_c) of the molecular received signal for each symbol slot is ignored (see Fig. 3 for the state diagram). In the rest of this paper, we call T_c as discarding time.
- Digital self-interference cancellation (D-SIC): we predict the number of SI molecules (i.e., the number of absorbed molecules originating from the unpaired transmitter) from the current bit and subtract it from the molecular received signal

Fig. 4 shows the full-duplex system with A-SIC and D-SIC. Note that the two SIC techniques can be applied separately. The channel coefficient of the system with A-SIC, $P_{ij}^\varphi[k]$, is given as follows:

$$P_{ij}^\varphi[k] = P_{ij}(kt_s + T_c, (k+1)t_s). \quad (8)$$

Hence, $N_{ij}[k]$ of the proposed two-way MCvD system with A-SIC is denoted by $N_{ij}^\varphi[k]$ and becomes

$$N_{ij}^\varphi[k] \sim \mathcal{B}(N_1, P_{ij}^\varphi[k]). \quad (9)$$

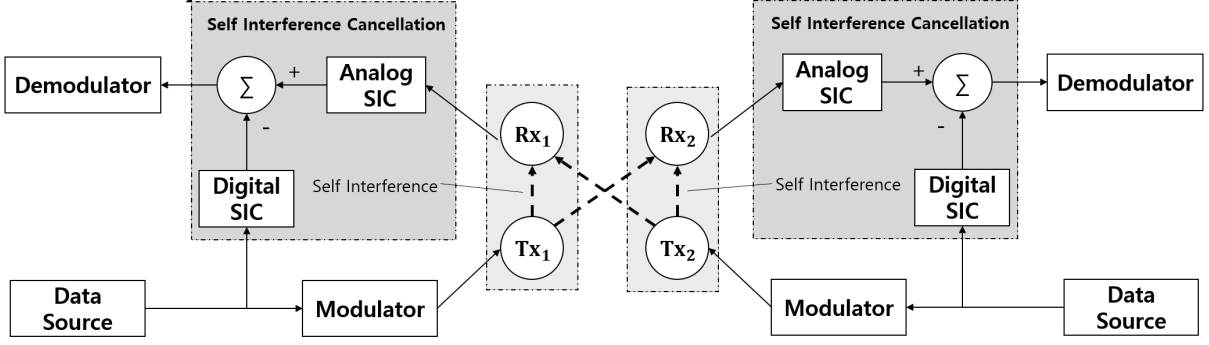


Fig. 4. Block diagram of the proposed two-way MCvD system with A-SIC and D-SIC.

Furthermore, $y_{\text{Rx}_j}[n]$ with A-SIC and D-SIC becomes

$$y_{\text{Rx}_j}^\varphi[n] \triangleq \sum_{k=0}^{n-1} (N_{ij}^\varphi[k] \cdot x_i[n-k] + \underbrace{N_{jj}^\varphi[k] \cdot x_j[n-k]}_{\text{self-interference}}) - \underbrace{\mathbb{E}[N_{jj}^\varphi[0] \cdot x_j[n]]}_{\text{when D-SIC applied}}, \quad (10)$$

where $\mathbb{E}[N_{jj}^\varphi[0] \cdot x_j[n]] = N_1 P_{jj}^\varphi[0] x_j[n]$.

$\mathbb{E}[\cdot]$ is the expectation operation. By applying these two SIC techniques, (7) is transformed into

$$y_{\text{Rx}_j}^\varphi[n] \sim \mathcal{N}(\mu_{n,\text{total}}^\varphi, (\sigma_{n,\text{total}}^\varphi)^2)$$

$$\mu_{n,\text{total}}^\varphi = \sum_{k=0}^{n-1} N_1 (P_{ij}^\varphi[k] x_i[n-k] + P_{jj}^\varphi[k] x_j[n-k]) - \underbrace{N_1 P_{jj}^\varphi[0] x_j[n]}_{\text{when D-SIC applied}}$$

$$(\sigma_{n,\text{total}}^\varphi)^2 = \sigma_{\text{noise}}^2 + \sum_{k=0}^{n-1} N_1 (P_{ij}^\varphi[k] (1 - P_{ij}^\varphi[k]) x_i[n-k] + P_{jj}^\varphi[k] (1 - P_{jj}^\varphi[k]) x_j[n-k]). \quad (11)$$

IV. CHANNEL MODEL & BER FORMULATION OF TWO-WAY MOLECULAR COMMUNICATION

We formulate the BER as a function of detection threshold τ , the number of molecules for encoding bit-1 (N_1), $P_{ij}^\varphi[k]$ ($P_{ij}^\varphi[k]$ when SIC is applied), and the symbol duration t_s . In this section, we first derive the channel model to obtain the channel coefficients (i.e., $P_{ij}^\varphi[k]$ and $P_{jj}^\varphi[k]$) and then utilize these channel coefficients in the BER calculations.

A. Channel Model

As we mentioned, the channel model is a time-dependent solution of the fraction of received molecules by time t . In the proposed two-way MCvD system, we cannot use (2) directly to derive the channel model since we have to consider the events of molecules being absorbed by each Rx_i , which are not independent of each other. The proposed BER formula and the SIC techniques are based on the channel model. However, there is no analytical closed-form solution in the literature

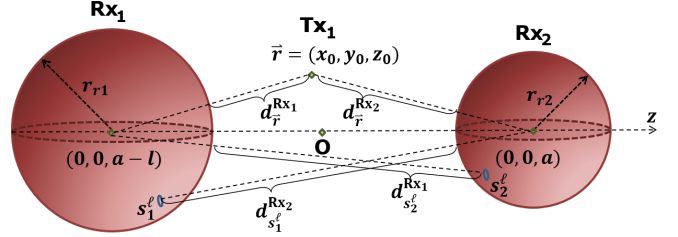


Fig. 5. Assumed topology in the derivation

for the case of two absorbing spherical receivers. In prior work on molecular MIMO [34], [35], researchers considered two pairs of point transmitters and fully absorbing receivers. To obtain the channel models, the authors in [34] and [35] utilized a one-way MCvD system channel model for a single receiver [18] and fitted the coefficients accordingly. In this paper, we propose a new approach to analytically derive the multi-receiver channel model.

Fig. 5 describes the notations and the cartesian coordinates in the derivation. The centers of two receivers are located on z -axis and the distance between them is denoted by ℓ (i.e., $(0, 0, a)$ and $(0, 0, a - \ell)$). Our goal is to obtain the fraction of received molecules by time t for the receivers when Tx_1 is the emitter (i.e., $F_1^{\text{Tx}_1}(t)$ and $F_2^{\text{Tx}_1}(t)$ for the receivers Rx_1 and Rx_2 , respectively).

In the rest of this subsection, we first derive a closed form of $\lim_{t \rightarrow \infty} F_1^{\text{Tx}_1}(t)$ and $\lim_{t \rightarrow \infty} F_2^{\text{Tx}_1}(t)$, which correspond to the probability that the molecule eventually being absorbed by Rx_1 and Rx_2 , respectively. This so-called asymptotic capture probability was studied in [36]. The authors in [36] derive an exact solution of the asymptotic capture probability for the case of two absorbing spheres, which has an identical radius. In this paper we generalize this solution to release the equal-radius constraint since our system adopts a general topology.

In the derivation of the asymptotic capture probability, we use bispherical coordinate (μ, η, ϕ) [37, p. 1298]). Note that bispherical coordinate is obtained by rotating bipolar axes about the line between the two foci, $(0, 0, \pm f)$ in cartesian

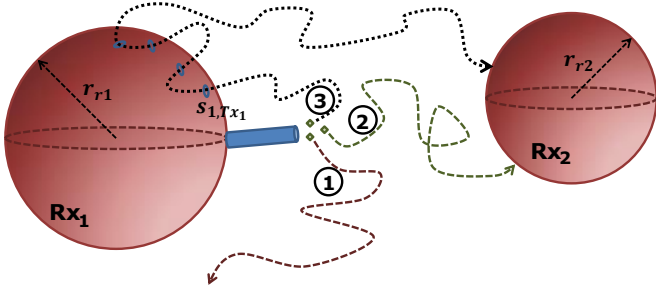


Fig. 6. Three possible traversal paths for a molecule emitted from Tx_1 . Path 1 corresponds to a molecule not hitting any of the receivers by time t . Path 2 corresponds to a molecule that is hitting the destination (Rx_2) at time t without hitting Rx_1 . Path 3 is a virtual path that corresponds to a molecule that is, actually hitting Rx_1 but that would hit Rx_2 at time t if Rx_1 was not in the environment or it was transparent to molecules.

coordinates:

$$\begin{aligned}\mu &= \tanh^{-1} \left(\frac{fz}{x^2 + y^2 + z^2 + (f/2)^2} \right), \\ \eta &= \tan^{-1} \left(\frac{f(x^2 + y^2)^{1/2}}{x^2 + y^2 + z^2 - (f/2)^2} \right), \\ \phi &= \tan^{-1} \left(\frac{y}{x} \right).\end{aligned}\quad (12)$$

Theorem 1. *The asymptotic capture probabilities in the cases of two receivers, i.e., $\lim_{t \rightarrow \infty} F_1^{Tx_1}(t)$ and $\lim_{t \rightarrow \infty} F_2^{Tx_1}(t)$, are as follows:*

$$\begin{aligned}\lim_{t \rightarrow \infty} F_1^{Tx_1}(t) &= \sqrt{2(\cosh \mu_0 - \cos \eta_0)} \\ &\times \left(\sum_{m=0}^{\infty} \frac{e^{-(m+\frac{1}{2})\mu_1} \sinh[(m+\frac{1}{2})(\mu_0 + \mu_2)]}{\sinh[(m+\frac{1}{2})(\mu_1 + \mu_2)]} P_m(\cos \eta_0) \right), \\ \lim_{t \rightarrow \infty} F_2^{Tx_1}(t) &= \sqrt{2(\cosh \mu_0 - \cos \eta_0)} \\ &\times \left(\sum_{m=0}^{\infty} \frac{e^{-(m+\frac{1}{2})\mu_2} \sinh[(m+\frac{1}{2})(\mu_1 - \mu_0)]}{\sinh[(m+\frac{1}{2})(\mu_1 + \mu_2)]} P_m(\cos \eta_0) \right)\end{aligned}\quad (13)$$

where $\mu_1 = \cosh^{-1} \left(\frac{\ell - a}{r_{r1}} \right)$ and $\mu_2 = \cosh^{-1} \left(\frac{a}{r_{r2}} \right)$, P_m is the m -th order Legendre polynomial, and (μ_0, η_0, ϕ_0) is the bispherical representation of the cartesian coordinate of Tx_1 (i.e., (x_0, y_0, z_0)) with two foci $(0, 0, \pm f)$,

$$f = r_{r2} \sinh \left(\cosh^{-1} \left(\frac{a}{r_{r2}} \right) \right).\quad (14)$$

Proof. Let $k_i(x_0, y_0, z_0)$ denotes an asymptotic capture probability for Rx_i , where $\vec{r} = (x_0, y_0, z_0)$ is the initial position of the molecule. The asymptotic capture probability satisfies the Laplace equation [38],

$$\begin{aligned}\nabla^2 k_1(\vec{r}) &= 0, \\ \nabla^2 k_2(\vec{r}) &= 0.\end{aligned}\quad (15)$$

The boundary conditions in this case are

$$k_1(\vec{r}) = 1, \quad k_2(\vec{r}) = 0 \quad \text{when} \quad d_{\vec{r}}^{Rx_1} = 0, \quad (16)$$

$$k_1(\vec{r}) = 0, \quad k_2(\vec{r}) = 1 \quad \text{when} \quad d_{\vec{r}}^{Rx_2} = 0, \quad (17)$$

$$k_1(\vec{r}), k_2(\vec{r}) \rightarrow 0 \quad \text{as} \quad d_{\vec{r}}^{Rx_1}, d_{\vec{r}}^{Rx_2} \rightarrow \infty, \quad (18)$$

where $d_{\vec{r}}^{Rx_1}$ and $d_{\vec{r}}^{Rx_2}$ is the distance from the initial point \vec{r} to Rx_1 and Rx_2 , respectively. Without loss of generality, we set a as follows:

$$a = \frac{\ell^2 + r_{r2}^2 - r_{r1}^2}{2\ell}, \quad (19)$$

By setting f and a as (14) and (19), the surface of Rx_1 and Rx_2 are represented as $\mu = \mu_1$ and $\mu = -\mu_2$, respectively. This enables us to utilize the typical solutions of the Laplace equation [37, p. 1299] and derive the solution of (15) as (13). \square

It can be easily shown that when $r_{r2} \rightarrow 0$, the asymptotic capture probability for Rx_2 (i.e., $\lim_{t \rightarrow \infty} F_2^{Tx_1}(t)$ in (13)) goes to 0 as $\mu_2 \rightarrow \infty$. Moreover, by using [37, eqs. (10.3.70)], we get the following:

$$\begin{aligned}\lim_{t \rightarrow \infty} F_1^{Tx_1}(t) &= \sqrt{\frac{\cosh \mu_0 - \cos \eta_0}{\cosh(\mu_0 - 2\mu_1) - \cos \eta_0}} \\ &= \frac{r_{r1}}{r_{r1} + d_{\vec{r}}^{Rx_1}}, \quad \text{when} \quad r_{r2} \rightarrow 0,\end{aligned}\quad (20)$$

which is the asymptotic capture probability for the single absorbing receiver case [18].

Based on the derived asymptotic capture probability, we provide a derivation of the approximation of the channel model. We investigate the multi-receiver channel model by considering the possible diffusion paths in the case of a two-way MCvD system. In Fig. 6, three possible traversal paths (diffusion paths) for a molecule emitted from Tx_1 are shown. $F_2^{Tx_1}(t)$ can be expressed as follows:

$$F_2^{Tx_1}(t) = \int_0^t f_2^{Tx_1}(t') dt', \quad (21)$$

where $f_2^{Tx_1}(t)$ denotes the instantaneous hitting probability density for the molecules following Path 2. Note that Tx_2 will not be considered in the derivation because we can obtain the whole case by superposition.

Remark 1. *Rx_1 will be regarded as a non-intended receiver on the path to Rx_2 and vice versa.*

Remark 2. *To obtain the probability corresponding to Path 2, we subtract the probability corresponding to Path 3 from the channel model of the one-way MCvD with a single point transmitter, which corresponds to the probability of $\{\text{Path 2} \cup \text{Path 3}\}$.*

Hence, we consider the instantaneous hitting probability densities for Rx_2 as follows:

$$f_2^{Tx_1}(t') = g_2^{Tx_1}(t') - \alpha(t'), \quad (22)$$

where $\alpha(t')$ corresponds to the instantaneous hitting probability densities for the molecules following Path 3. Additionally, $g_2^{Tx_1}(t')$ corresponds to the single receiver case that is given in the literature as (2), i.e., the union of Path 2 and Path 3 as if Rx_1 is not in the environment. Therefore, if we calculate $\alpha(t')$, then we can calculate $f_2^{Tx_1}(t')$, which in turn will lead us to $F_2^{Tx_1}(t')$.

By definition, each of the molecules that is moving through Path 3 visits R_{X_1} at least once. Therefore, we can segment Path 3 into two parts. For those molecules originating from T_{X_1} , we denote the first hitting point on the surface of R_{X_1} as $s_{1,T_{X_1}}$ and the corresponding first hitting time as τ . Note that $s_{1,T_{X_1}}$ can be an arbitrary point on the surface of R_{X_1} and τ can be any real value less than t' .

The instantaneous hitting probability density for $s_{1,T_{X_1}}$ on the surface of R_{X_1} (i.e., the arrival time distribution for $s_{1,T_{X_1}}$ when the molecules are emitted from T_{X_1}) is denoted by $f_1^{T_{X_1}}(t', s_{1,T_{X_1}})$. Since $s_{1,T_{X_1}}$ is the first hitting point on the surface of R_{X_1} , it can be regarded as the starting point of the successive path to R_{X_2} . Hence, (22) can be rewritten as

$$f_2^{T_{X_1}}(t') = g_2^{T_{X_1}}(t') - \int_0^{t'} \int_{\Omega_1} f_1^{T_{X_1}}(\tau, s_{1,T_{X_1}}) g_2^{s_{1,T_{X_1}}}(t' - \tau) ds_{1,T_{X_1}} d\tau, \quad (23)$$

where Ω_1 indicates the points on the surface of R_{X_1} . To obtain $f_2^{T_{X_1}}(t')$, we also need to consider $f_1^{T_{X_1}}(t')$ in a similar way. Thus, we have the following:

$$f_1^{T_{X_1}}(t') = g_1^{T_{X_1}}(t') - \int_0^{t'} \int_{\Omega_2} f_2^{T_{X_1}}(\tau, s_{2,T_{X_1}}) g_1^{s_{2,T_{X_1}}}(t' - \tau) ds_{2,T_{X_1}} d\tau, \quad (24)$$

where $s_{2,T_{X_1}}$ is the first hitting point on R_{X_2} that is analogous to $s_{1,T_{X_1}}$ for R_{X_1} .

When we apply the mean value theorem for integration to the surface integration in (23), we get

$$f_2^{T_{X_1}}(t') = g_2^{T_{X_1}}(t') - \int_0^{t'} g_2^{s'_1(t', \tau)}(t' - \tau) \int_{\Omega_1} f_1^{T_{X_1}}(\tau, s_{1,T_{X_1}}) ds_{1,T_{X_1}} d\tau, \quad (25)$$

where $s'_1(t', \tau)$ is a point $\in \Omega_1$. After the surface integration in (25), we obtain

$$f_2^{T_{X_1}}(t') = g_2^{T_{X_1}}(t') - \int_0^{t'} g_2^{s'_1(t', \tau)}(t' - \tau) f_1^{T_{X_1}}(\tau) d\tau. \quad (26)$$

In the same way, we can express $f_1^{T_{X_1}}(t')$ as

$$f_1^{T_{X_1}}(t') = g_1^{T_{X_1}}(t') - \int_0^{t'} g_1^{s'_2(t', \tau)}(t' - \tau) f_2^{T_{X_1}}(\tau) d\tau, \quad (27)$$

where $s'_2(t', \tau)$ is a point $\in \Omega_2$.

Note that to derive $s'_i(t', \tau)$ requires the closed forms of $f_i^{T_{X_1}}(t)$, therefore, it is unattainable to solve the simultaneous equations (26) and (27). Therefore, we set $s'_i(t', \tau)$ as a constant $s_i^\ell \in \Omega_i$, and then derive the approximation of $f_i^{T_{X_1}}(t)$ by solving (26) and (27). We determine the two constants s_1^ℓ and s_2^ℓ by matching the asymptotic values of approximation forms and (13). By substituting $s'_i(t', \tau)$ with s_i^ℓ and integrating (26) and (27), we obtain the following:

$$\begin{aligned} F_2^{T_{X_1}}(t) &= G_2^{T_{X_1}}(t) - \int_0^t g_2^{s_1^\ell}(t') * f_1^{T_{X_1}}(t') dt' \\ F_1^{T_{X_1}}(t) &= G_1^{T_{X_1}}(t) - \int_0^t g_1^{s_2^\ell}(t') * f_2^{T_{X_1}}(t') dt'. \end{aligned} \quad (28)$$

Then, we get

$$\begin{aligned} F_2^{T_{X_1}}(t) &= G_2^{T_{X_1}}(t) - g_2^{s_1^\ell}(t) * F_1^{T_{X_1}}(t) \\ F_1^{T_{X_1}}(t) &= G_1^{T_{X_1}}(t) - g_1^{s_2^\ell}(t) * F_2^{T_{X_1}}(t). \end{aligned} \quad (29)$$

Next, we take $t \rightarrow \infty$ in (28), which gives us

$$\begin{aligned} \lim_{t \rightarrow \infty} F_2^{T_{X_1}}(t) &= \lim_{t \rightarrow \infty} G_2^{T_{X_1}}(t) - \lim_{t \rightarrow \infty} G_2^{s_1^\ell}(t) \lim_{t \rightarrow \infty} F_1^{T_{X_1}}(t) \\ \lim_{t \rightarrow \infty} F_1^{T_{X_1}}(t) &= \lim_{t \rightarrow \infty} G_1^{T_{X_1}}(t) - \lim_{t \rightarrow \infty} G_1^{s_2^\ell}(t) \lim_{t \rightarrow \infty} F_2^{T_{X_1}}(t), \end{aligned} \quad (30)$$

In (30), $G_2^{s_1^\ell}(t)$ and $G_1^{s_2^\ell}(t)$ are expressed as follows:

$$\begin{aligned} G_2^{s_1^\ell}(t) &= \frac{r_{r2}}{r_{r2} + d_{s_1^\ell}^{R_{X_2}}} \operatorname{erfc} \left(\frac{d_{s_1^\ell}^{R_{X_2}}}{\sqrt{4Dt}} \right) \\ G_1^{s_2^\ell}(t) &= \frac{r_{r1}}{r_{r1} + d_{s_2^\ell}^{R_{X_1}}} \operatorname{erfc} \left(\frac{d_{s_2^\ell}^{R_{X_1}}}{\sqrt{4Dt}} \right), \end{aligned} \quad (31)$$

where $d_{s_1^\ell}^{R_{X_2}}$ is the distance from s_1^ℓ to R_{X_2} , and $d_{s_2^\ell}^{R_{X_1}}$ is the distance from s_2^ℓ to R_{X_1} . By solving (30) simultaneously, we obtain

$$\begin{aligned} \lim_{t \rightarrow \infty} F_2^{T_{X_1}}(t) &= \lim_{t \rightarrow \infty} \frac{G_2^{T_{X_1}}(t) - G_2^{s_1^\ell}(t) G_1^{T_{X_1}}(t)}{1 - G_2^{s_1^\ell}(t) G_1^{s_2^\ell}(t)} \\ \lim_{t \rightarrow \infty} F_1^{T_{X_1}}(t) &= \lim_{t \rightarrow \infty} \frac{G_1^{T_{X_1}}(t) - G_1^{s_2^\ell}(t) G_2^{T_{X_1}}(t)}{1 - G_2^{s_1^\ell}(t) G_1^{s_2^\ell}(t)}. \end{aligned} \quad (32)$$

We obtain $d_{s_1^\ell}^{R_{X_2}}$ and $d_{s_2^\ell}^{R_{X_1}}$ from the fact that (13) is equal to (32) (See Appendix A).

Finally, we derive the approximation forms of $F_1^{T_{X_1}}(t)$ and $F_2^{T_{X_1}}(t)$ based on (29), as follows (see Appendix B):

$$\begin{aligned} F_i^{T_{X_1}}(t) &= \frac{-c_{i,1}}{\sqrt{\pi t}} \sum_{n=-1}^{-\infty} \left[\left\{ (A^n - 1) \left(\frac{d_{T_{X_1}}^{R_{X_i}}}{\sqrt{D}} - u \right) + \frac{B}{(A-1)} (nA^{n+1} \right. \right. \\ &\quad \left. \left. - (n+1)A^{n+1} \right\} e^{-\frac{u^2}{4t}} + (A^n - 1) \sqrt{\pi t} \operatorname{erf} \left(\frac{u}{\sqrt{4t}} \right) \right] \frac{d_{T_{X_1}}^{R_{X_i}}}{\sqrt{D}} + nB \\ &\quad + \frac{c_{i,2}}{\sqrt{\pi t}} \sum_{n=-1}^{-\infty} \left[\left\{ (A^n - 1) (b_i - u) + \frac{B}{(A-1)} (nA^{n+1} \right. \right. \\ &\quad \left. \left. - (n+1)A^{n+1} \right\} e^{-\frac{u^2}{4t}} + (A^n - 1) \sqrt{\pi t} \operatorname{erf} \left(\frac{u}{\sqrt{4t}} \right) \right] \frac{b_i + nB}{b_i + (n+1)B}, \end{aligned} \quad (33)$$

$$\begin{aligned} \text{where } A &= \frac{(r_{r1} + d_{s_2^\ell}^{R_{X_1}})(r_{r2} + d_{s_1^\ell}^{R_{X_2}})}{r_{r1} r_{r2}}, \quad B = - \left(\frac{d_{s_1^\ell}^{R_{X_2}} + d_{s_2^\ell}^{R_{X_1}}}{\sqrt{D}}, \right. \\ b_1 &= \left(\frac{d_{s_2^\ell}^{R_{X_1}} + d_{T_{X_1}}^{R_{X_2}}}{\sqrt{D}}, \right) \quad b_2 = \left(\frac{d_{s_1^\ell}^{R_{X_2}} + d_{T_{X_1}}^{R_{X_1}}}{\sqrt{D}}, \right) \\ c_{1,1} &= \frac{Ar_{r1}}{(A-1)(r_{r1} + d_{T_{X_1}}^{R_{X_1}})}, \quad c_{1,2} = \frac{Ar_{r1} r_{r2}}{(A-1)(r_{r2} + d_{T_{X_1}}^{R_{X_2}})(r_{r1} + d_{s_2^\ell}^{R_{X_1}})}, \\ c_{2,1} &= \frac{Ar_{r2}}{(A-1)(r_{r2} + d_{T_{X_1}}^{R_{X_2}})}, \quad c_{2,2} = \frac{Ar_{r1} r_{r2}}{(A-1)(r_{r1} + d_{T_{X_1}}^{R_{X_1}})(r_{r2} + d_{s_1^\ell}^{R_{X_2}})}, \text{ and} \\ [H(u)]_b^a &= H(a) - H(b). \end{aligned}$$

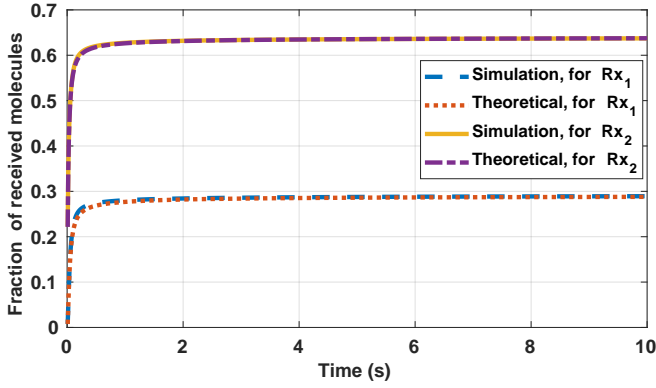


Fig. 7. A comparison of the theoretical fraction of received molecules with the simulation data ($d_1=d_2=1.5 \mu\text{m}$).

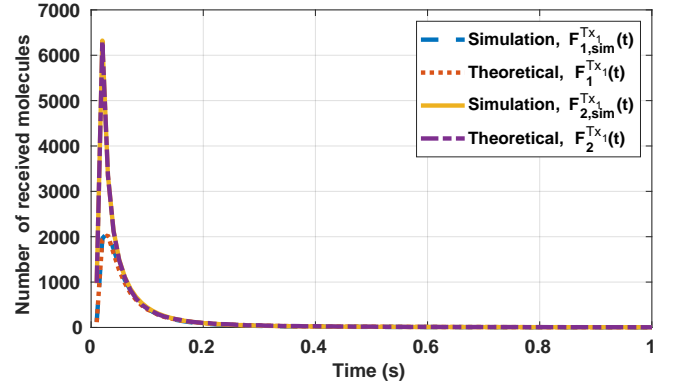


Fig. 8. A comparison of the theoretical number of received molecules with the simulation data ($d_1=d_2=1.5 \mu\text{m}$).

TABLE I
SIMULATION PARAMETERS FOR CHANNEL MODEL VERIFICATION

System Parameter	Notation	Values
Distance (Tx_i to Rx_i)	d_1	$1.5 \mu\text{m}$
Distance (Tx_i to Rx_j)	$d_{\text{Tx}_i}^{\text{Rx}_j}$	$5 \mu\text{m} - d_1$
Number of Molecules for Bit 1	N_1	50000
Diffusion Coefficient	D	$100 \mu\text{m}^2/\text{s}$
Radius of Receiver	$r_{r1}=r_{r2}$	$5 \mu\text{m}$
Simulation Time Step	Δt	10^{-5}s
Simulation Duration		0.1 s
Simulation Replication		10
Number of the terms in (13) and (33)	m, n	100000

B. Channel Model Verification

In this Section, we verify our channel model by particle-based simulation. We repeat the simulation for a number of times, and take the mean value with respect to the number of trials. The number of trials is presented in Tables II and III. In each simulated trial, 50000 molecules are released. The received molecules are distinguished according to the transmitter that emits them. In the simulations, only Tx_1 releases molecules which is sufficient to verify the theoretical channel model.

To implement Brownian motion for the emitted molecules, our simulator records and updates the position of each molecule at each time step Δt . The position of the emitted molecules, $\mathbf{X}_p(t)$, changes by $\Delta \mathbf{X}_p$ after simulation time step Δt as in (34) [39]. The simulation parameters used for verification of the channel model are given in Table I.

$$\begin{aligned} \mathbf{X}_p(t + \Delta t) &= \mathbf{X}_p(t) + \Delta \mathbf{X}_p \\ &= \mathbf{X}_p(t) + (\Delta x, \Delta y, \Delta z) \end{aligned} \quad (34)$$

$$\Delta x, \Delta y, \Delta z \sim \mathcal{N}(0, 2D\Delta t).$$

Through extensive simulations, we obtain the fraction of received molecules for each receiver (i.e., Rx_1 and Rx_2) at each time step during the simulation time, i.e., $F_{2,\text{sim}}^{\text{Tx}_1}(t)$ and $F_{1,\text{sim}}^{\text{Tx}_1}(t)$, respectively. Then, we use (33) to calculate $F_2^{\text{Tx}_1}(t)$ and $F_1^{\text{Tx}_1}(t)$. We compare the analytical results with the simulation results, as shown in Fig. 7. It is worth noting that the asymptotic capture probabilities (i.e., $\lim_{t \rightarrow \infty} F_1^{\text{Tx}_1}(t)$ and $\lim_{t \rightarrow \infty} F_2^{\text{Tx}_1}(t)$ in (13)) for Fig. 7 are 0.6414 and 0.2932,

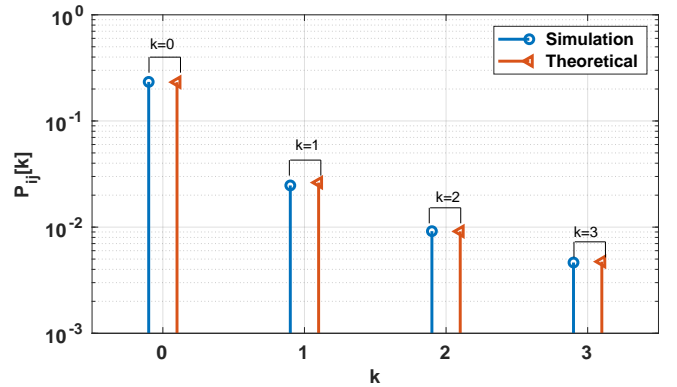


Fig. 9. A comparison of the theoretical channel coefficients with the simulation data ($t_s = 0.150 \text{ s}$, $d_1=d_2=1.5 \mu\text{m}$, $r_{r1}=r_{r2}=5 \mu\text{m}$).

respectively. By the long-term simulation (i.e., $t = 1000\text{s}$), we observe that the simulation results and (33) converge to those values. We depict the number of received molecules in Fig. 8, which corresponds to the impulse response of the channel. Theoretical values in Fig. 8 at $t = k\Delta t$ are obtained by calculating

$$N_1 (F_i^{\text{Tx}_1}((k+1)\Delta t) - F_i^{\text{Tx}_1}(k\Delta t)). \quad (35)$$

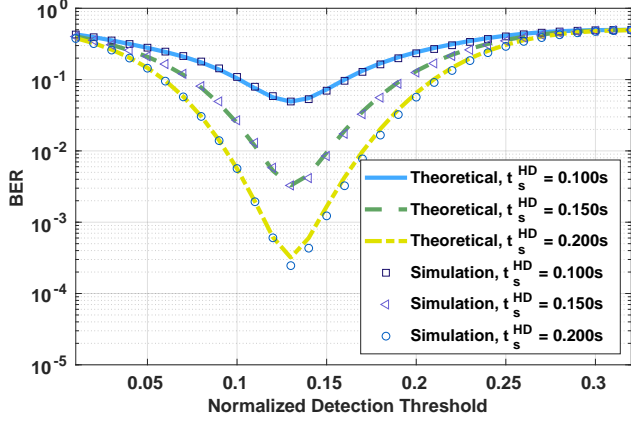
Using the derived channel model, we substitute $P_{ij}[k]$ and $P_{ij}^\varphi[k]$ as follows:

$$\begin{aligned} P_{ij}[k] &= F_j^{\text{Tx}_i}((k+1)t_s) - F_j^{\text{Tx}_i}(kt_s), \\ P_{ij}^\varphi[k] &= F_j^{\text{Tx}_i}((k+1)t_s) - F_j^{\text{Tx}_i}(kt_s + T_c). \end{aligned} \quad (36)$$

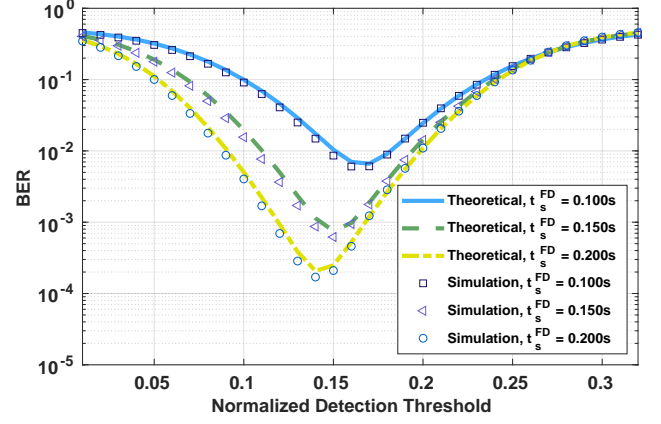
In Fig. 9, we depict the comparison of the channel coefficients $P_{ij}[k]$.

C. BER Formula for Two-Way Molecular Communication

In this section, we formulate the BER in terms of the Q-function (i.e., the tail probability of the standard normal distribution). For the receiver Rx_j , an error occurs when the result of decoding is different from the bit transmitted from the Tx_i . If Tx_i encodes bit-1, an error occurs when $y_{\text{Rx}_j}[n]$ is less than the detection threshold τ_d . If Tx_i encodes bit-0,



(a) Half-duplex system



(b) Full-duplex system

Fig. 10. (a) BER comparison of the simulation data and the theoretical analysis of the half-duplex system using BCSK (b) BER comparison of the simulation data and the theoretical analysis of the full-duplex system with D-SIC ($N_1=500$, $d_1=d_2=1.5 \mu\text{m}$, $r_{r1}=r_{r2}=5 \mu\text{m}$).

TABLE II
SIMULATION PARAMETERS FOR BER AND THROUGHPUT COMPARISON

System Parameter	Notation	Values
Distance (Tx _i to Rx _i)	$d_1=d_2$	1.5 μm
Distance (Tx _i to Rx _j)	$d_{\text{Tx}_1}^{\text{Rx}_2}=d_{\text{Tx}_2}^{\text{Rx}_1}$	5 $\mu\text{m}-d_1$
Number of Molecules for Bit 1	N_1	300, 400, 500
Diffusion Coefficient	D	100 $\mu\text{m}^2/\text{s}$
Radius of Receiver	r_r	5 μm
Simulation Time Step	Δt	10 ⁻⁵ s
Molecular Noise Variance	σ_{noise}^2	100
Considered ISI Period		0.6s
Number of the terms in (13) and (33)	m, n	100000
Replication		10

then an error occurs when $y_{\text{Rx}_j}[n]$ is greater than the detection threshold τ_d .

Considering the transmitted bit sequences x_i and x_j , we obtain the error probabilities at the n th symbol slot as (37) where $x_i[1:n-1]$ denotes the bits transmitted previously from Tx_i:

$$\begin{aligned}
 P_e^{j,BCSK} &= P_{e,x_i[n]=1}^{j,BCSK} + P_{e,x_i[n]=0}^{j,BCSK} \\
 &= \sum_{x_i[1:n-1]} \sum_{x_j} P_{i,1} P(y_{\text{Rx}_j}[n] \leq \tau_d | x_i[n]=1, x_i, x_j) \\
 &+ \sum_{x_i[1:n-1]} \sum_{x_j} P_{i,0} P(y_{\text{Rx}_j}[n] > \tau_d | x_i[n]=0, x_i, x_j) \\
 &= \sum_{x_i[1:n-1]} \sum_{x_j} P_{i,1} Q \left(\frac{\mu_{n,\text{total}} | x_i, x_j - \tau_d}{\sigma_{n,\text{total}} | x_i, x_j} \right) \\
 &+ \sum_{x_i[1:n-1]} \sum_{x_j} P_{i,0} Q \left(\frac{\tau_d - \mu_{n,\text{total}} | x_i, x_j}{\sigma_{n,\text{total}} | x_i, x_j} \right), \quad (37)
 \end{aligned}$$

where $\mu_{n,\text{total}}$ and $\sigma_{n,\text{total}}^2$ are defined in (7), $Q(\cdot)$ is the Q-function, and

$$\begin{aligned}
 P_{i,1} &= P(x_i[n]=1) P(x_i[1:n-1]) P(x_j[1:n]) \\
 P_{i,0} &= P(x_i[n]=0) P(x_i[1:n-1]) P(x_j[1:n]). \quad (38)
 \end{aligned}$$

Note that $\sum_{x_i[1:n-1]}$ and \sum_{x_j} in (37) indicate the summation over all possible bit sequences $x_i[1:n-1]$ and $x_j[1:n]$, respectively. The BER expression for the full-duplex system with the proposed SIC techniques is obtained by substituting $y_{\text{Rx}_j}[n]$, $\mu_{n,\text{total}} | x_i, x_j$ and $\sigma_{n,\text{total}}^2 | x_i, x_j$ in (38) with $y_{\text{Rx}_j}^\varphi[n]$, $\mu_{n,\text{total}}^\varphi | x_i, x_j$, and $(\sigma_{n,\text{total}}^\varphi)^2$, respectively.

V. PARTICLE-BASED SIMULATION RESULTS

In this section, we compare the proposed half-duplex and full-duplex systems in terms of BER and throughput. Throughput of the systems are evaluated as follows:

$$\text{Throughput} = \frac{M(1 - P_e)}{t_s}, \quad (39)$$

where M is the number of bits transmitted in one symbol, P_e is the BER of the system, and t_s denotes the symbol duration. The system parameters for the rest of our work are summarized in Table II. For convenience, we denote t_s of the half-duplex and full-duplex systems as t_s^{HD} and t_s^{FD} , respectively. In Table III and Table IV, throughput ratio is calculated as a ratio of the throughput of full-duplex system and the half-duplex system.

In the half-duplex system, each receiver operates only when the paired transmitter releases the molecular signal. Hence, the operating time of the receiver (i.e., detection period) is half of the symbol duration. In the full-duplex system, the detection period of each receiver is equal to the symbol duration. Roughly, we can expect faster but less accurate communications in the full-duplex system if we use the same modulation technique and detection period for both systems. By the theoretical and simulation BER analysis, we confirm that the proposed SIC techniques are necessary in the full-duplex system. Therefore we analyze the BER improvement in the full-duplex system with SIC to find, numerically, the optimal values for the normalized detection threshold and the discarding time of the SIC to minimize BER. Through the numerical parameter optimization, the throughput of the full-duplex system with SIC is compared to the half-duplex

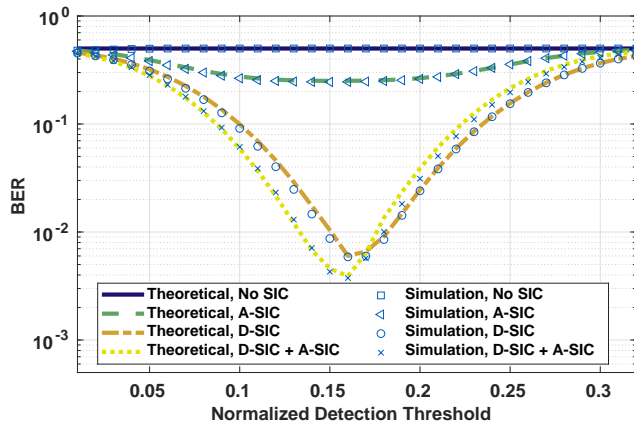


Fig. 11. BER of the full-duplex system with the different SIC techniques ($N_1=500$, $t_s^{\text{FD}}=0.1\text{s}$, $r_{r1}=r_{r2}=5\text{ }\mu\text{m}$). For the no-SIC case, we set $d_1=d_2=0\text{ }\mu\text{m}$. For other cases, we set $d_1=d_2=1.5\text{ }\mu\text{m}$.

system. For a fair comparison, we evaluate the throughput in the following three cases, considering that the throughput is a function of M , t_s , and P_e :

- 1) Half-duplex system (BCSK) vs. full-duplex system (BCSK) with SIC, where $t_s^{\text{FD}}=t_s^{\text{HD}}/2$.
- 2) Half-duplex system (BCSK) vs. full-duplex system (BCSK) with SIC. We set the same t_s for both systems (i.e., $t_s^{\text{FD}}=t_s^{\text{HD}}$).
- 3) Half-duplex system (BCSK) vs. full-duplex system (BCSK) with SIC. We empirically adjust t_s^{FD} to make the BER of both systems close.
- 4) Half-duplex system using quadrature concentration shift keying (QCSK) vs full-duplex system (BCSK) with SIC, where $t_s^{\text{FD}}=t_s^{\text{HD}}/2$.

A. BER Analysis

Fig. 10(a) depicts the simulation and theoretical BERs of the half-duplex system using BCSK. The x -axis is the normalized threshold (τ_m), which is τ_d/N_1 . First of all, the simulation and theoretical values match each other well. Since the half-duplex system is not susceptible to SI, we do not need to apply the proposed SIC techniques to this system. On the other hand, we observe from Fig. 11 that the BER of the full-duplex system is nearly 0.3 if we do not apply the SIC techniques. In Fig. 10(a), we can see the optimal normalized threshold τ_m^* for different t_s^{HD} and we observe that it is slightly changing according to the value of t_s^{HD} . We also observe that the BER gain is relatively higher for changing t_s^{HD} from 0.100 s to 0.150 s compared to from 0.150 s to 0.200 s due to the relative ISI difference.

Fig. 10(b) shows the simulation and theoretical BER of the full-duplex system with D-SIC. We can see that there is an optimal normalized detection threshold τ_m^* for different t_s^{FD} values. Similar to the case of the half-duplex system, there is some similarity between the τ_m^* changes according to the t_s^{FD} value and also the tendency of the BER gain with respect to the t_s^{FD} difference (see Fig. 10(a)).

Fig. 11 depicts the simulation and theoretical BERs of the full-duplex system while applying the different SIC techniques. The x -axis is the normalized detection threshold

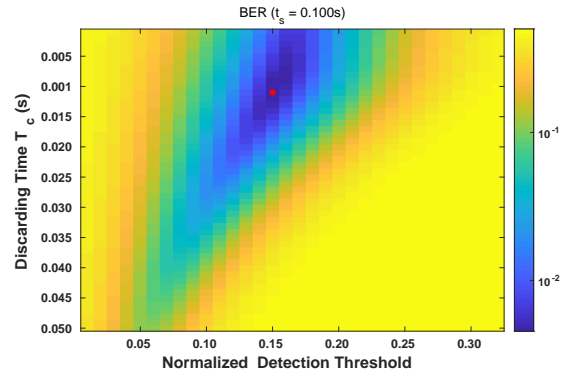


Fig. 12. Theoretical BER heatmap of the full-duplex system with A-SIC and D-SIC. The red mark indicates the optimal parameters for the normalized detection threshold and the discarding time.

τ_d/N_1 . The performance of D-SIC is superior to the performance of A-SIC, because D-SIC deals with a wider time interval (i.e., when the discarding time is T_c , A-SIC ignores the molecules received in $[0, T_c]$, and D-SIC subtracts the expected number of the SI molecules received in $[T_c, t_s]$). For the no-SIC case, we assume that Tx_i is located on the surface of Rx_i (i.e., $d_1=d_2=0\text{ }\mu\text{m}$), and we observe that the BER is nearly 0.5. The results indicate that the separation of transmitter and receiver is necessary in the two-way MCvD system. We observe that the BER of the full-duplex system with A-SIC is nearly 0.3. On the other hand, the BER of the full-duplex system with D-SIC becomes comparable with the half-duplex system in Fig.10(a). Moreover, we observe that when we apply both SIC techniques, the BER is slightly improved compared to the full-duplex system with only D-SIC. As we stated in (7) and (11), the number of received SI molecules from the current symbol can be modeled as a Gaussian random variable that has a variance $N_1 P_{ii}^\varphi[0](1 - P_{ii}^\varphi[0])x_i[n]$. Since the variance decreases as $P_{ii}^\varphi[0]$ decreases (when $P_{ii}^\varphi[0] \leq 0.5$), applying A-SIC can reduce the uncertainty of predicting the number of received SI molecules from the current symbol. For the full-duplex systems, since the BER of the A-SIC-only system and the no-SIC system are not reasonable, we consider those full-duplex systems with only D-SIC or D-SIC and A-SIC.

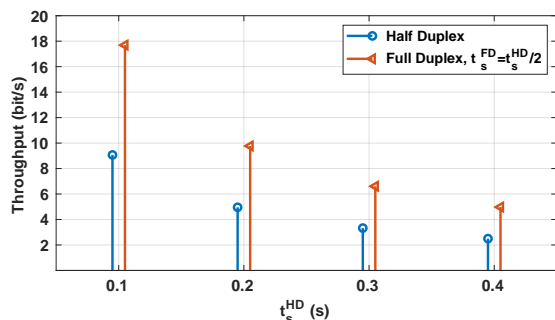
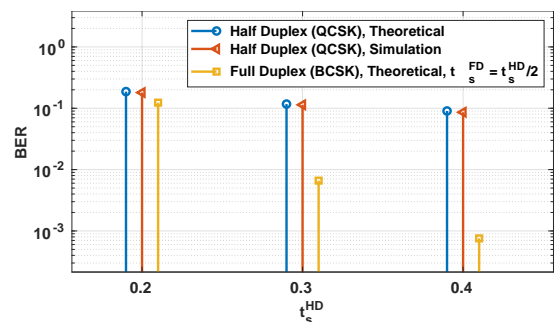
As derived in Section IV, the BER is a function of symbol duration (t_s), detection threshold (τ_d), the number of molecules for encoding bit-1 (N_1), and the discarding time of molecular received signal for A-SIC (T_c). Since N_1 and t_s are system parameters, we consider only τ_d and T_c as variables to optimize. While we will show that optimal values for these parameters exist, we cannot derive them in closed-form and hence must resort to evaluating them numerically. To improve BER, we first need to see the structure of the BER of the full-duplex system with SIC in terms of τ_d and T_c by the following analysis.

In Fig. 12, we depict a heatmap of the theoretical BER with respect to T_c and τ_m for the full-duplex system with D-SIC and A-SIC. We observe that τ_m minimizing the BER with given T_c decreases as T_c increases. It is because that the molecules from the paired transmitter (i.e., desired signal) are also discarded by A-SIC. For each t_s^{FD} , we find global

TABLE III

THROUGHPUT RATIO (FD/HD), t_s AND BER VALUES OF THE HALF-DUPLEX SYSTEM USING BCSK AND THE FULL-DUPLEX SYSTEM USING BCSK.

		$N_1 = 300$				$N_1 = 400$				$N_1 = 500$			
		0.100 s	0.200 s	0.300 s	0.400 s	0.100 s	0.200 s	0.300 s	0.400 s	0.100 s	0.200 s	0.300 s	0.400 s
Case 1	$t_s^{\text{HD}} = 2t_s^{\text{FD}}$	0.100 s	0.200 s	0.300 s	0.400 s	0.100 s	0.200 s	0.300 s	0.400 s	0.100 s	0.200 s	0.300 s	0.400 s
	BER (FD)	0.1155	0.0229	0.0083	0.0045	0.0887	0.0097	0.0022	0.0009	0.0721	0.0045	6.7×10^{-4}	1.9×10^{-4}
	BER (HD)	0.0931	0.0086	0.0022	0.0010	0.0660	0.0017	0.0002	5×10^{-5}	0.0492	3.1×10^{-4}	1.5×10^{-5}	1.5×10^{-6}
	THP Ratio	1.9506	1.9711	1.9876	1.9929	1.9515	1.9840	1.9959	1.9983	1.9517	1.9916	1.9987	1.9996
Case 2	$t_s^{\text{FD}} = t_s^{\text{HD}}$	0.100 s	0.200 s	0.300 s	0.400 s	0.100 s	0.200 s	0.300 s	0.400 s	0.100 s	0.200 s	0.300 s	0.400 s
	BER (FD)	0.0229	0.0045	0.0023	0.0014	0.0097	0.0009	0.0003	0.0001	0.0045	1.9×10^{-4}	4.7×10^{-5}	1.1×10^{-5}
	BER (HD)	0.0931	0.0086	0.0022	0.0010	0.0660	0.0017	0.0002	5×10^{-5}	0.0492	3.1×10^{-4}	1.5×10^{-5}	1.5×10^{-6}
	THP Ratio	1.0774	1.0041	0.9999	0.9997	1.0603	1.0008	0.9999	0.9999	1.0469	1.0001	1.0000	1.0000
Case 3	t_s^{HD}	0.100 s	0.200 s	0.300 s	0.400 s	0.100 s	0.200 s	0.300 s	0.400 s	0.100 s	0.200 s	0.300 s	0.400 s
	t_s^{FD}	0.056 s	0.147 s	0.320 s	0.630 s	0.056 s	0.165 s	0.390 s	2.785 s	0.056 s	0.178 s	0.398 s	N/A
	THP Ratio	1.7747	1.3603	0.9375	0.6349	1.7853	1.2122	0.7692	0.1436	1.7820	1.1236	0.7538	N/A

Fig. 13. Theoretical BER of the half-duplex system (BCSK) and the full-duplex system with optimized D-SIC and A-SIC (BCSK), where $t_s^{\text{FD}} = t_s^{\text{HD}}/2$.Fig. 14. Theoretical and simulation BER of the half-duplex system (QCSK) and the theoretical BER of the full-duplex system with optimized D-SIC and A-SIC (BCSK), N_1 is 500.

optimal normalized detection threshold and the discarding time in order to minimize the BER and denote them as red mark on the heatmap. We utilized these optimal values in the SIC algorithm to compare the throughput of the half-duplex system and the full-duplex system with SIC.

As was mentioned before, for comparison, we consider the following three cases: i) set $t_s^{\text{FD}} = t_s^{\text{HD}}/2$ (to observe a trade off between the throughput and BER); ii) set the same t_s for both systems; iii) fix t_s^{HD} and adjust t_s^{FD} empirically to make the BER of both systems close. For the case iii), adjusted t_s^{FD} values are in Table III.

For the case i), Fig. 13 shows that the throughputs of the

TABLE IV
THROUGHPUT RATIO (FD/HD) OF THE HALF-DUPLEX SYSTEM USING QCSK AND THE FULL-DUPLEX SYSTEM USING BCSK WITH OPTIMIZED D-SIC AND A-SIC

N_1	t_s^{HD} (s)	t_s^{FD} (s)	Throughput Ratio (FD/HD)
300	0.200	0.100	1.222
	0.300	0.150	1.295
	0.400	0.200	1.274
400	0.200	0.100	1.134
	0.300	0.150	1.188
	0.400	0.200	1.162
500	0.200	0.100	1.078
	0.300	0.150	1.125
	0.400	0.200	1.098

full-duplex system with optimized SIC are almost double the throughput of the half-duplex system. Thus, we can achieve nearly double the transmission rate using the proposed SIC techniques without degrading the BER significantly. When $t_s^{\text{HD}} = t_s^{\text{FD}}$ is 0.100 s or 0.200 s, the BER of the full-duplex system with optimized SIC is less than the BER of the half-duplex system. The converse is true when $t_s^{\text{HD}} = t_s^{\text{FD}}$ is 0.300 s or 0.400 s. Adjusted t_s^{FD} throughput values in Table III show the same tendency. The overall results imply that the full-duplex system with optimized SIC becomes better than the half-duplex system even in terms of BER when t_s get decreased.

In Fig. 14 we depict the simulation and theoretical BER of the half-duplex system using QCSK and compare them to the full-duplex system with optimized SIC using BCSK where $t_s^{\text{FD}} = t_s^{\text{HD}}/2$. In this case, M/t_s is the same for both systems. Hence, the BER determines the difference between the throughputs. For QCSK, we used an equally spaced number of molecules for encoding different bits (i.e., bit-0, 1, 2, 3) and three thresholds (i.e., τ_{d1} , τ_{d2} , τ_{d3}) to detect the molecular received signal. Fig. 14 shows that the BER of the half-duplex system using QCSK is much higher than that of the full-duplex system using BCSK with optimized SIC. The theoretical BERs of the half-duplex system using QCSK are calculated by using a straightforward extension of (37). The throughput difference between the two systems can be seen in Table IV.

VI. CONCLUSION

In this paper, we have investigated two different communication models of two-way MCvD—a half-duplex system and a full-duplex system. We derived the multi-receiver channel model. We also derived the BER formula and verified the formula by simulation. Theoretical analysis and simulations showed that severe SI occurs in the full-duplex system. Therefore, we proposed two SIC techniques to mitigate this interference: A-SIC and D-SIC. We analyzed the BER improvements in the full-duplex system with the proposed SIC techniques and numerically found the optimal values for the normalized detection threshold and the discarding time in order to minimize the system BER. To compare the half-duplex system with the full-duplex system, we evaluated the throughput in three different cases. The throughput of the full-duplex system with optimized SIC increased to more than that of the half-duplex system as t_s decreased. With the proposed SIC techniques, we showed the possibility of full-duplex molecular communication using a single type of molecule. On the other hand, the BER analysis and simulation results revealed that using a concentration-based modulation technique of higher order significantly degrades the BER. Investigating a more effective modulation technique for the two-way MCvD will be a topic for the future work. We will also study the channel model for more general system configurations.

VII. APPENDIX

A. Derivation of $d_{s_1^{\ell}}^{\text{Rx}_2}$ and $d_{s_2^{\ell}}^{\text{Rx}_1}$

Using (2), we rewrite (30) and combine with (13) as

$$k_1 = \lim_{t \rightarrow \infty} F_1^{\text{Tx}_1}(t) = \frac{\frac{r_{r1}}{r_{r1}+d_{\text{Tx}_1}^{\text{Rx}_1}} - \frac{r_{r1}}{r_{r1}+d_{s_2^{\ell}}^{\text{Rx}_1}} - \frac{r_{r2}}{r_{r2}+d_{\text{Tx}_1}^{\text{Rx}_2}}}{1 - \frac{r_{r2}}{r_{r2}+d_{s_1^{\ell}}^{\text{Rx}_2}} - \frac{r_{r1}}{r_{r1}+d_{s_2^{\ell}}^{\text{Rx}_1}}}, \quad (40)$$

$$k_2 = \lim_{t \rightarrow \infty} F_2^{\text{Tx}_1}(t) = \frac{\frac{r_{r2}}{r_{r2}+d_{\text{Tx}_1}^{\text{Rx}_2}} - \frac{r_{r2}}{r_{r2}+d_{s_1^{\ell}}^{\text{Rx}_2}} - \frac{r_{r1}}{r_{r1}+d_{\text{Tx}_1}^{\text{Rx}_1}}}{1 - \frac{r_{r2}}{r_{r2}+d_{s_1^{\ell}}^{\text{Rx}_2}} - \frac{r_{r1}}{r_{r1}+d_{s_2^{\ell}}^{\text{Rx}_1}}},$$

where k_1 and k_2 indicate $k_1(\mu, \eta, \phi)$ and $k_2(\mu, \eta, \phi)$, respectively. Note that (40) can be rewritten as quadratic equations of $d_{s_1^{\ell}}^{\text{Rx}_2}$ and $d_{s_2^{\ell}}^{\text{Rx}_1}$, and the solutions of the equations are derived as the following:

$$d_{s_1^{\ell}}^{\text{Rx}_2} = \frac{r_{r2}^2(k_1 + k_2 - 1) + r_{r2}d_{\text{Tx}_1}^{\text{Rx}_2}(k_1 + k_2)}{r_{r2}(1 - k_2) - d_{\text{Tx}_1}^{\text{Rx}_2}k_2} \quad (41)$$

$$d_{s_2^{\ell}}^{\text{Rx}_1} = \frac{r_{r1}^2(k_1 + k_2 - 1) + r_{r1}d_{\text{Tx}_1}^{\text{Rx}_1}(k_1 + k_2)}{r_{r1}(1 - k_1) - d_{\text{Tx}_1}^{\text{Rx}_1}k_1}.$$

B. Derivation of (33)

Through performing Laplace transform in (29) and solving simultaneous equations, we get

$$F_2^{\text{Tx}_1}(s) = \frac{-(A-1)c_1e^{-b_1\sqrt{\frac{s}{D}}}}{s(e^{B\sqrt{\frac{s}{D}}} - A)} + \frac{(A-1)c_2e^{-b_2\sqrt{\frac{s}{D}}}}{s(e^{B\sqrt{\frac{s}{D}}} - A)}$$

$$F_1^{\text{Tx}_1}(s) = \frac{-(A-1)c_3e^{-b_3\sqrt{\frac{s}{D}}}}{s(e^{B\sqrt{\frac{s}{D}}} - A)} + \frac{(A-1)c_4e^{-b_4\sqrt{\frac{s}{D}}}}{s(e^{B\sqrt{\frac{s}{D}}} - A)}, \quad (42)$$

where $F_2^{\text{Tx}_1}(s)$ and $F_1^{\text{Tx}_1}(s)$ are the Laplace transform of $F_2^{\text{Tx}_1}(t)$ and $F_1^{\text{Tx}_1}(t)$, respectively. To derive the inverse Laplace transforms of (42), we first derive the inverse Laplace transforms of $F_2^{\text{Tx}_1}(s^2)$ and $F_1^{\text{Tx}_1}(s^2)$, where

$$F_2^{\text{Tx}_1}(s^2) = \frac{-(A-1)c_1e^{-\frac{b_1s}{\sqrt{D}}}}{s^2(e^{\frac{Bs}{\sqrt{D}}} - A)} + \frac{(A-1)c_2e^{-\frac{b_2s}{\sqrt{D}}}}{s^2(e^{\frac{Bs}{\sqrt{D}}} - A)} \quad (43)$$

$$F_1^{\text{Tx}_1}(s^2) = \frac{-(A-1)c_3e^{-\frac{b_3s}{\sqrt{D}}}}{s^2(e^{\frac{Bs}{\sqrt{D}}} - A)} + \frac{(A-1)c_4e^{-\frac{b_4s}{\sqrt{D}}}}{s^2(e^{\frac{Bs}{\sqrt{D}}} - A)}.$$

Using [40, eqs. (5.1), (5.57), (1.18)], the inverse Laplace transforms of (43) can be expressed as the following:

$$L^{-1}\{F_2^{\text{Tx}_1}(s^2)\} = k_3(t) - k_4(t) \quad (44)$$

$$L^{-1}\{F_1^{\text{Tx}_1}(s^2)\} = k_1(t) - k_2(t),$$

where

$$k_i(t) = u(t-b_i) \left\{ \frac{A^n-1}{A-1}(t-b_i) + \frac{B(-nA^{n+1}+(n+1)A^n-1)}{(A-1)^2} \right\},$$

$$b_i + (n+1)B < t < b_i + nB, n = -1, -2, \dots -\infty. \quad (45)$$

In (45), $u(t)$ is the unit step function. From (45), we derive the inverse Laplace transform of (42) as the following [40, eqs. (1.27)]:

$$F_2^{\text{Tx}_1}(t) = \frac{1}{2\sqrt{\pi t^3}} \int_0^\infty ue^{-\frac{u^2}{4t}} (L^{-1}\{F_2^{\text{Tx}_1}(s^2)\}) du \quad (46)$$

$$F_1^{\text{Tx}_1}(t) = \frac{1}{2\sqrt{\pi t^3}} \int_0^\infty ue^{-\frac{u^2}{4t}} (L^{-1}\{F_1^{\text{Tx}_1}(s^2)\}) du,$$

which give us (33).

REFERENCES

- [1] J. W. Kwack, H. B. Yilmaz, N. Farsad, C.-B. Chae, and A. Goldsmith, "Two way molecular communications," in *Proc. ACM Int. Conf. Nanoscale Comput. Commun. (NANOCOM)*, Sep. 2018.
- [2] D. A. LaVan, T. McGuire, and R. Langer, "Small-scale systems for in vivo drug delivery," *Nat. Biotechnol.*, vol. 21, no. 10, pp. 1184–1191, Oct. 2003.
- [3] A. A. G. Requicha, "Nanorobots, NEMS, and nanoassembly," *Proc. IEEE*, vol. 91, no. 11, pp. 1922–1933, Nov. 2003.
- [4] S. Basu, Y. Gerchman, C. H. Collins, F. H. Arnold, and R. Weiss, "A synthetic multicellular system for programmed pattern formation," *Nature*, vol. 434, no. 7037, pp. 1130–1134, Apr. 2005.
- [5] A. Cavalcanti and R. A. Freitas-Jr., "Nanorobotics control design: a collective behavior approach for medicine," *IEEE Trans. Nanobiosci.*, vol. 4, no. 2, pp. 133–140, Jun. 2005.
- [6] P. Couvreur and C. Vauthier, "Nanotechnology: Intelligent design to treat complex disease," *Springer Pharmaceut. Res.*, vol. 23, no. 7, pp. 1417–1450, Jun. 2006.

- [7] N. Farsad, H. B. Yilmaz, A. Eckford, C.-B. Chae, and W. Guo, "A comprehensive survey of recent advancements in molecular communication," *IEEE Commun. Surveys Tuts.*, vol. 18, no. 3, pp. 1887–1919, Oct. 2016.
- [8] W. Guo, C. Mias, N. Farsad, and J.-L. Wu, "Molecular versus electromagnetic wave propagation loss in macro-scale environments," *IEEE Trans. Mol. Biol. Multi-Scale Commun.*, vol. 1, no. 1, pp. 18–25, Mar. 2015.
- [9] D. Malak and O. B. Akan, "Molecular communication nanonetworks inside human body," *Elsevier Nano Commun. Netw.*, vol. 3, no. 1, pp. 19–35, Mar. 2012.
- [10] M. S. Kuran, H. B. Yilmaz, T. Tugcu, and B. Zerman, "Energy model for communication via diffusion in nanonetworks," *Nano Communication Networks*, vol. 1, no. 2, Jul. 2010.
- [11] T. Danino, O. Mondragón-Palomino, L. Tsimring, and J. Hasty, "A synchronized quorum of genetic clocks," *Nature*, vol. 463, no. 7279, pp. 326–330, Jan. 2010.
- [12] A. Prindle, P. Samayoa, I. Razinkov, T. Danino, L. Tsimring, and J. Hasty, "A sensing array of radically coupled genetic biopixels," *Nature*, vol. 481, pp. 39–44, Jan. 2012.
- [13] H. B. Kaplan and E. P. Greenberg, "Diffusion of autoinducer is involved in regulation of the vibrio fischeri luminescence system," *J. Bacteriol.*, vol. 163, no. 3, pp. 1210–1214, Sep. 1985.
- [14] A. Einolghozati, M. Sardari, A. Beirami, and F. Fekri, "Data gathering in networks of bacteria colonies: Collective sensing and relaying using molecular communication," in *Proc. IEEE Int. Conf. on Comput. Commun. Workshops (INFOCOM WKSHPs)*, Mar. 2012.
- [15] S. Redner, *A guide to first-passage processes*. Cambridge University Press, Aug. 2001.
- [16] K. V. Srinivas, A. W. Eckford, and R. S. Adve, "Molecular communication in fluid media: The additive inverse gaussian noise channel," *IEEE Trans. Inf. Theory*, vol. 58, no. 7, pp. 4678–4692, Dec. 2012.
- [17] T. Nakano, Y. Okaie, and J.-Q. Liu, "Channel model and capacity analysis of molecular communication with brownian motion," *IEEE Commun. Lett.*, vol. 16, no. 6, pp. 797–800, Jun. 2012.
- [18] H. B. Yilmaz, A. C. Heren, T. Tugcu, and C.-B. Chae, "Three-dimensional channel characteristics for molecular communications with an absorbing receiver," *IEEE Commun. Lett.*, vol. 18, no. 6, pp. 929–932, Apr. 2014.
- [19] G. Genc, Y. E. Kara, H. B. Yilmaz, and T. Tugcu, "ISI-aware modeling and achievable rate analysis of the diffusion channel," *IEEE Commun. Lett.*, vol. 20, no. 9, pp. 1729–1732, Jun. 2016.
- [20] A. Noel, K. C. Cheung, and R. Schober, "Improving receiver performance of diffusive molecular communication with enzymes," *IEEE Trans. Nanobiosci.*, vol. 13, no. 1, pp. 31–43, Mar. 2014.
- [21] B. Tepekule, A. E. Pusane, H. B. Yilmaz, C.-B. Chae, and T. Tugcu, "ISI mitigation techniques in molecular communication," *IEEE Trans. Mol. Biol. Multi-Scale Commun.*, vol. 1, no. 2, pp. 202–216, Jun. 2015.
- [22] D. Bharadia, E. McMillin, and S. Katti, "Full duplex radios," *SIGCOMM Comput. Commun. Rev.*, vol. 43, no. 4, pp. 375–386, Aug. 2013.
- [23] E. Everett, A. Sahai, and A. Sabharwal, "Passive self-interference suppression for full-duplex infrastructure nodes," *IEEE Trans. Wireless Commun.*, vol. 13, no. 2, pp. 680–694, Feb. 2014.
- [24] M. Chung, M. S. Sim, J. Kim, K. Kim, Dong, and C.-B. Chae, "Prototyping real-time full duplex radios," *IEEE Commun. Mag.*, vol. 53, no. 9, pp. 56–63, Sep. 2015.
- [25] A. E. P. Bayram Cevdet Akdeniz and T. Tugcu, "Two-way communication systems in molecular communication," in *Proc. IEEE Int. Black Sea Conf. on Commun. and Netw. (BlackSeaCom)*, Jun. 2017.
- [26] Y. Huang, M. Wen, C. Lee, C.-B. Chae, and F. Ji, "A two-way molecular communication assisted by an impulsive force," *IEEE Trans. Ind. Informat.*, vol. 15, no. 5, pp. 3048–3057, May 2019.
- [27] M. Farahnak-Ghazani, G. Aminian, M. Mirmohseni, A. Gohari, and M. Nasiri-Kenari, "On medium chemical reaction in diffusion-based molecular communication: A two-way relaying example," *IEEE Trans. Commun.*, vol. 67, no. 2, pp. 1117–1132, Feb. 2019.
- [28] N.-R. Kim and C.-B. Chae, "Novel modulation techniques using isomers as messenger molecules for nano communication networks via diffusion," *IEEE J. Sel. Areas Commun.*, vol. 31, no. 12, pp. 847–856, Dec. 2013.
- [29] N.-R. Kim, A. Eckford, and C.-B. Chae, "Symbol interval optimization for molecular communication with drift," *IEEE Trans. Nanotechnol.*, vol. 13, no. 3, pp. 223–229, Jul. 2014.
- [30] N.-R. Kim, N. Farsad, A. Eckford, and C.-B. Chae, "Channel and noise models for nonlinear molecular communication systems," *IEEE J. Sel. Areas Commun.*, vol. 32, no. 12, pp. 2392–2401, Dec. 2014.
- [31] N. Farsad, W. Guo, and A. Eckford, "Tabletop molecular communication: Text messages through chemical signals," *PLoS one*, vol. 8, no. 12, p. e82935, Dec. 2013.
- [32] H. Shahmohammadian, G. G. Messier, and S. Magierowski, "Blind synchronization in diffusion-based molecular communication channels," *IEEE Commun. Lett.*, vol. 17, no. 11, pp. 2156–2159, Nov. 2013.
- [33] J. V. Tyrrell and K. Harris, *Diffusion in Liquids: A Theoretical and Experimental Study*, Jan. 1984, vol. 5.
- [34] B. H. Koo, C. Lee, H. B. Yilmaz, N. Farsad, A. Eckford, and C.-B. Chae, "Molecular MIMO: From theory to prototype," *IEEE J. Sel. Areas Commun.*, vol. 34, no. 3, pp. 600–614, Mar. 2016.
- [35] C. Lee, H. B. Yilmaz, C.-B. Chae, N. Farsad, and A. Goldsmith, "Machine learning based channel modeling for molecular MIMO communications," in *Proc. IEEE Workshop on Signal Process. Adv. in Wireless Commun. (SPAWC)*, Apr. 2017.
- [36] H. Sano, "Solutions to the Smoluchowski equation for problems involving the anisotropic diffusion or absorption of a particle," *Chemical Physics - CHEM PHYS*, vol. 74, pp. 1394–1400, 01 1981.
- [37] P. M. Morse and H. Feshbach, *Methods of theoretical physics*, 1953.
- [38] M. Tachiya, "General method for calculating the escape probability in diffusion-controlled reactions," *The Journal of Chemical Physics*, vol. 69, no. 6, pp. 2375–2376, 1978.
- [39] H. B. Yilmaz and C.-B. Chae, "Simulation study of molecular communication systems with an absorbing receiver: Modulation and ISI mitigation techniques," *Simulation Modelling Practice and Theory*, vol. 49, pp. 136–150, Dec. 2014.
- [40] F. Oberhettinger and L. Harris, Badii, *Tables of Laplace Transforms*, 1973.